

UnderOak Observer

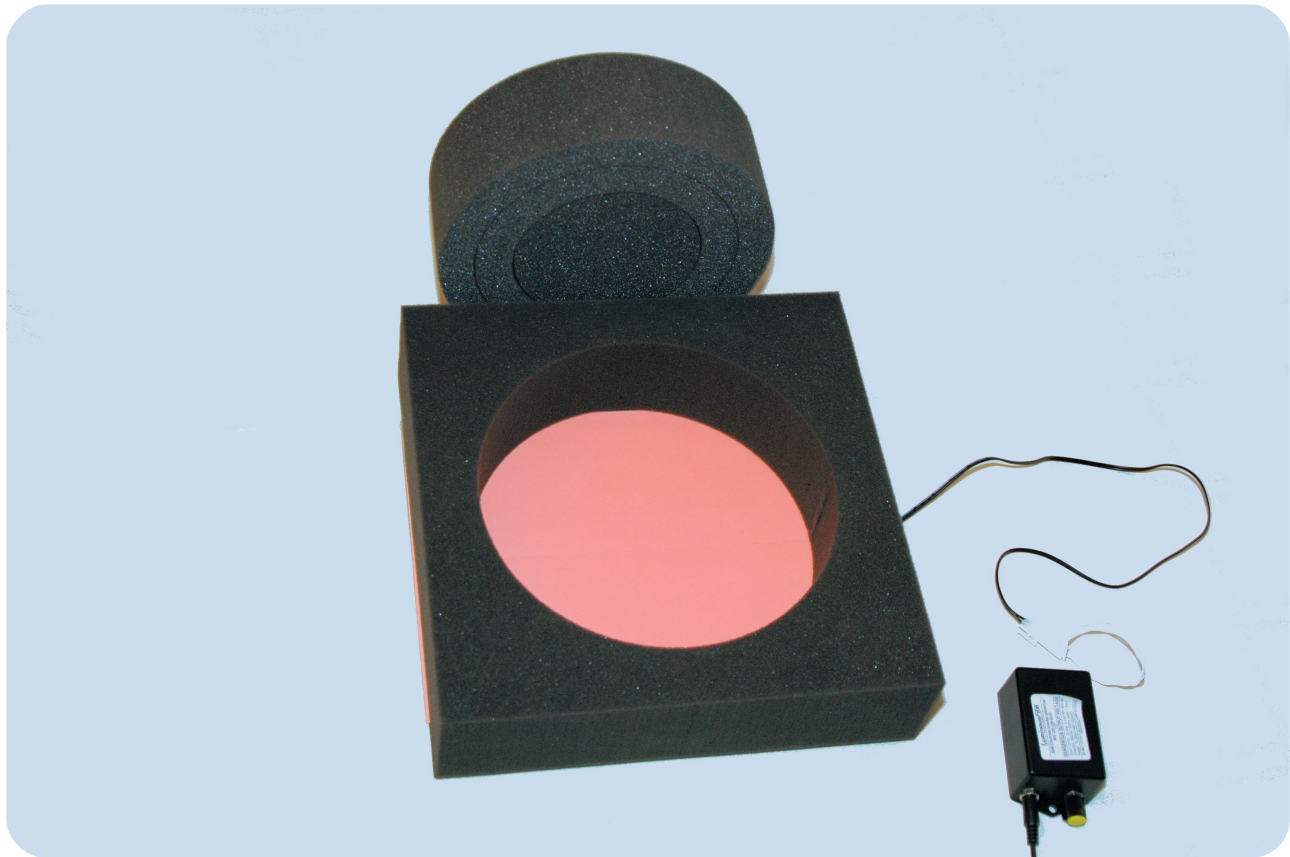
Issue 1 · July - September 2011

Photometry Basics - Part I

**Photometric & Period Analysis of
the Eclipsing Binary OO Aquila**

Building a Lite ELPH for Flat-fielding

▶ Cover Art: vdB 93 - RGB color simulated from DSS plates



A Lite ELPH for Flat-fielding a CCD Camera

I must confess up front that much of what will be described below started as a potential commercial venture about six months ago. As such the final product which I intended to call the “Lite ELPH” is a reasonably refined assemblage of off-the-shelf parts and one optional custom made item. There is nothing particularly brilliant about its implementation. In a large sense it is a consolidation of many ideas

bantered about on many astronomy-based websites and therefore wholly unpatentable. Nonetheless, completion of this project was an educational adventure into cost containment and free-market forces which I found nearly as interesting as its actual design. In the end, the projected cost even with steep volume discounts for individual components did not offer any significant advantage over similar products presently on the

market. This account is therefore offered free of charge to anyone who prefers to build rather than buy. I therefore assume no responsibility for any trouble you may get into with your significant other or injuries sustained from improper handling of this high voltage electrical device. Also, I have absolutely no personal, commercial or financial ties to any of the vendors which are mentioned in this article.

The collection of proper CCD flat-fields represents one of the more challenging tasks in lowering the noise floor necessary to extract the last bit of detail out of an image. Flats are intended to capture the fixed noise signature which may include out of focus artifacts from dust aka “donuts”, imperfections on the CCD matrix, and any other uneven illumination such as that caused by optical vignetting. Any change to the optical train, including filters, orientation or cleanliness will require the collection of new flats. Ideally, not unlike taking bias and dark frames, this should be a highly controlled process but for many amateur astrophotographers this goal falls short for a variety of reasons. The narrow window of opportunity at dawn or dusk is rarely long enough particularly if one needs to collect twilight flats and flat darks from multiple filters. Skylight flats which require averaging dozens of images simply take too long. Some folks swear by them, but in my hands, daytime “T-shirt” flats never achieve the level of uniformity expected from flats. Another option includes the construction of a home-made light

box featuring a diffused indirect incandescent or white LED light source. Most examples I’ve seen employ a complicated array of diffusers or lights, are bulky, not particularly portable, and often only address the needs of a single telescope. By comparison, designing a light weight box around an electroluminescent panel (ELP) greatly simplifies the design parameters. A single device can easily cover all apertures between 3 and 8” which is fortuitous since this likely represents the largest market segment for amateur astronomers. As such, most of the assembly details described below focuses on telescopes in this size range but is scalable to the many different sizes commercially available (A2-A6).

Technology from the 1960s

ELP technology has been around for at least five decades and most commonly used to backlight instrument panels or displays for a broad range of products (e.g. watches, automobile dashboards, nightlights, ad signs). Not all ELPs are created equally so that the selection process deserves special attention. I’ll leave it up to the reader to Google the product specifications on ELPs, but in a nutshell it is important to make sure that the output spectrum is as broad as possible between 400-700nm. This is particularly important to ensure sufficient output signal for those folks using narrow band filters. At least one ELP (FLATLITE®) would appear to meet this requirement based upon

Caveats:

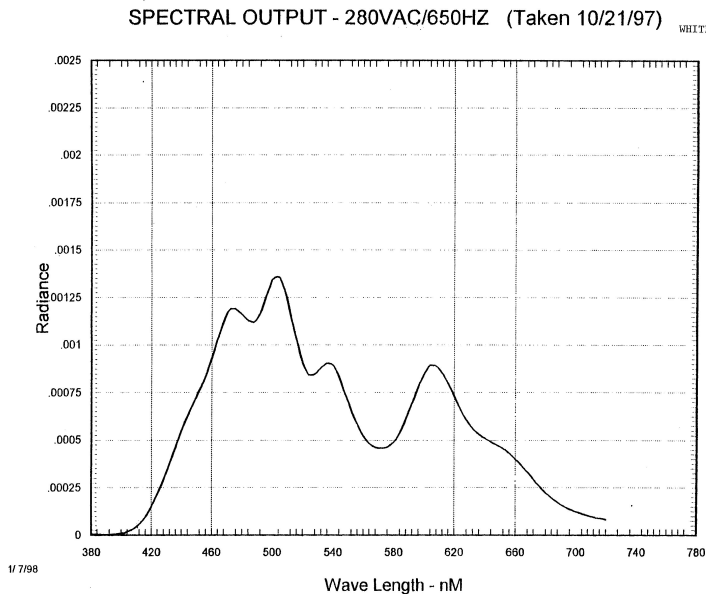
The "UnderOak Observer" is published advertisement free using Scribus (v1.3.3.14). Its intent is both entertainment and informational. Every reasonable effort is made to verify facts and avoid personal bias, however, the reader bears full responsibility for actually listening to what I have to say.



Cover Page Art:

van den Bergh 93 reflection and emission nebula in Canis Major. Color was rendered using Registar after synthesizing green from red and blue images downloaded with the DSS Plate Finder (http://archive.stsci.edu/cgi-bin/dss_plate_finder).

Editor: Kevin B. Alton
Writer: Kevin B. Alton



Above (Fig. 2)
Spectral output from
FLATLITE© split-electrode
ELP

Bottom right (Fig. 3)
Illuminated split-electrode
ELP shown seam

their published spectrum (<http://www.e-lite.com>). More about this later on when the spectral output from two different ELP lamps collected under real world conditions will be revealed. This particular spectrum (Fig. 2) comes from a 9"×12" split-electrode panel (pink off – white on) purchased from Knema, LLC (<http://www.luminousfilm.com/category/Electroluminescent-Panel+-Inverter-24>). There is, however, a seam down the middle of the panel (Fig. 3) which is clearly visible but interestingly does not appear in any clear or photometric B, V or I_c filter flats taken (n=20) with an SBIG ST402-ME camera.

Each EL panel is imbedded in a plastic laminate but for the most part, these light sources are not designed for continual use outside and should be stored away from direct sunlight (UV is damaging), excessive heat, and moisture. Outdoor and UV resistant laminates are available as custom

ordered items but at considerable added cost. Lamp brightness is dependent on the input voltage and frequency. Most of the ELPs suitable for flat-fielding require the purchase of a DC power supply and a DC/AC inverter. They both must be carefully matched to the ELP surface area to provide optimal illumination and lamp lifetime. The inverter can produce very high voltage (50-350 VAC) with an applied frequency between 50 Hz to 3 KHz so that care must be taken in handling these devices. A 12 VDC@1 amp wall-wart power supply and a dimmable 100 VAC@ 600 Hz split electrode inverter were purchased as a bundled package with the 9"×12" ELP described above for less than the price of individual components. Dimmable inverters are a good investment since there is a significant advantage in being able to adjust the amount of light needed to obtain 30-50% of the full-well capacity of a CCD camera over an appropriate period of time.

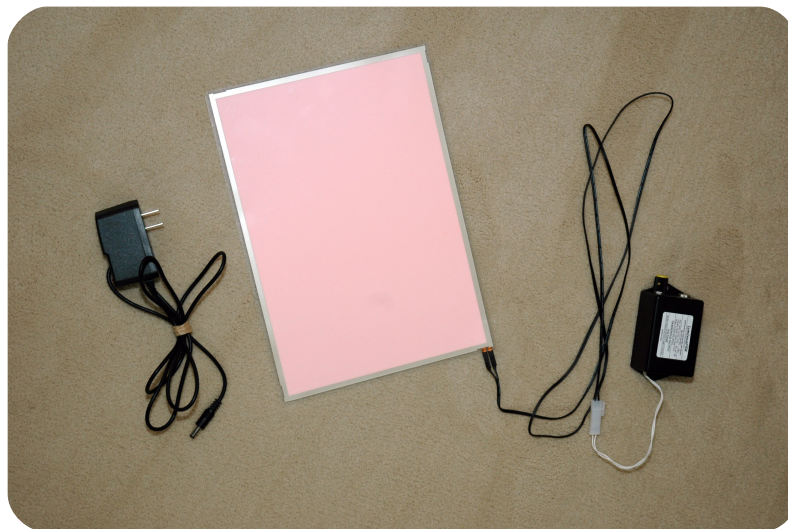
For those concerned about the seam visible with the split-electrode configuration, there is also a parallel



electrode electroluminescent lamp (Fig. 3) which is generally available in many of the same sizes (A2 to A6). Please note that these dimensions do not necessarily correspond to the illuminated portion of the panel. Unfortunately, for instance, an A4 sized panel which is nominally 11.7×8.3 inches does not provide a large enough illuminated surface (~11.25×7.88") to entirely fill up the image field from an 8" telescope. An A3-sized ELP would accommodate up to 11" whereas an A2-sized panel will fully illuminate a 16" telescope. It is possible to get custom sizes but the cost will escalate significantly unless you plan on ordering a large number for a group or club. Larger panels can be cut to size (<http://www.luminousfilm.com/tech/fabrication-sheet-se-.pdf>) however this is not a job for the faint-hearted since each cut edge must be resealed to prevent moisture invasion or a short-circuit.

OK, let's build this thing

Enough said about the ELP light source and onto actually constructing a light box to take flat-field images. EL panels are too thin (~0.02") and flimsy to be used without additional support. A good solution to this problem is to sandwich an ELP between two appropriately sized sheets of acrylic plastic. Clear or frosted Plexiglass (aka Lucite and Perspex) can be purchased at your local Home Depot or Lowes; however, the internet offers a greater variety in sizes, colors and thicknesses. There are many vendor choices but eStreetPlastics

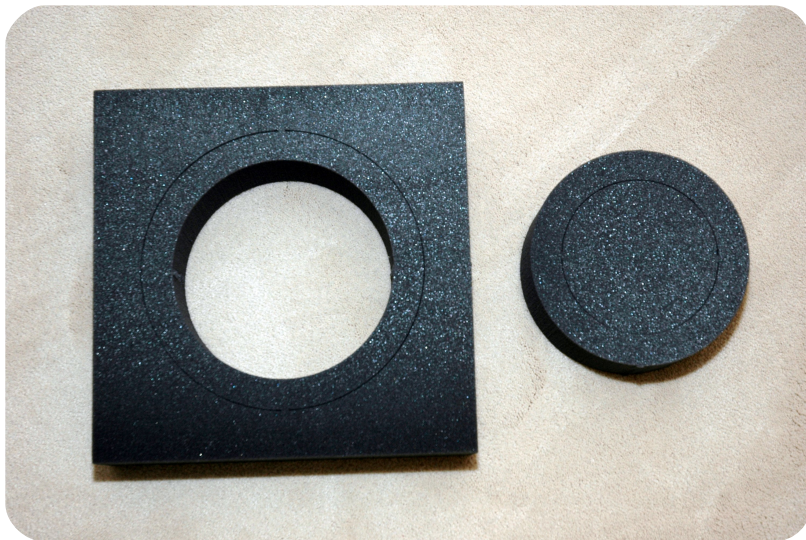


(<http://www.estreetplastics.com/>) probably has one of the best selections of sizes and colors. Since my largest telescope has 8" of aperture, the stock 12"×12"×1/8" sheets were perfectly suited to my needs. Compared to frosted Plexiglass, white Plexiglass with the same thickness (1/8") was very effective at attenuating (10% vs 70%) the lamp output. Interestingly, frosted Plexiglass was not much different than a clear acrylic sheet. Functionally it probably doesn't matter, but I chose black for the bottom piece of the sandwich based largely on esthetic preference. The next consideration is how to fasten the pieces together. I shied away from directly gluing them together since there was concern regarding compatibility with Plexiglass and potential seepage into the laminate protecting the EL panel. One viable option would be to drill holes in the Plexiglass at a number of strategically located positions outside the ELP perimeter and fasten the sandwich using appropriately sized nylon

Above (Fig. 3)
Size A4 parallel electrode ELP
with 12V DC power supply and
inverter

Raison d'être...

This marks the first of what I hope to be many issues of the "UnderOak Observer" published on a quarterly basis. Although this inaugural issue is also focused on a do-it-yourself project I've called the "Lite ELPH", I expect that most issues will be heavily oriented towards the photometric research on variable stars and minor planets that is regularly conducted from UnderOak, my backyard observatory. The organization of each Research Article will follow a format similar to that expected in peer reviewed papers. However, in contrast to rigid formalism there will be a generous supply of sidebar comments or tips which will hopefully clarify new concepts and encourage other amateur astronomers to consider participating in this exciting research.



Above (Fig. 4)
Charcoal black foam block
with pre-cut concentric
circles to accommodate
different aperture
telescopes

screws and nuts (e.g. 1/4-20 and 3/8" length). Non metallic fasteners are probably a better choice since they are not electrically conductive and shouldn't scratch any surface they may inadvertently contact. Another alternative is to seal the periphery using rubber or Neoprene U shaped edge trim (1/4" opening) such as those available at McMaster's (<http://www.mcmaster.com/#trim-molding/=c8dkwf>). FWIW, U-shaped door edge trim available at your local auto parts store is unfortunately not wide enough to accommodate two 1/8" acrylic sheets.

For many folks, assembly can stop at this point since the device is ready to mount on the wall or position directly on top of an optical tube. Conversely, the more elegant design I had in mind from the beginning of this project included a foam shroud pre-cut with concentric circles (5, 7 and 9") which would accommodate most telescopes with 4", 6" or 8" of aperture (Fig. 4). I reasoned that without a shroud, the user would have to position the

telescope perfectly level pointing upwards rather than being able to fit it in any orientation. Furthermore, since not all telescopes necessarily have a flush flat surface to balance a flat panel, a shroud could provide more flexibility and security. The overall size of the charcoal foam (firm) custom ordered from Foam N' More, Inc. (<http://www.foamforyou.com/>) was 12"×12"×3". The three concentric circles are not cut fully around; each features two narrow tabs in a staggered configuration which can be easily sliced away with a knife or scissors. This pick-and-cut approach affords additional rigidity should the user only be interested fitting a single telescope. Since I have already paid the setup charge to have these foam blocks fabricated, anyone interested in obtaining the exact same item should be able to purchase them without incurring that initial fee. Check with the folks at Foam N' More before ordering anything since I am making some assumptions in this regard. Perhaps the cleverest contribution made to the overall design of this shrouded light-box involves the use of snap-in panel fasteners (aka ChristmasTree™ clips) to lock the Plexiglass-ELP sandwich together and to provide multiple posts (Fig. 5) onto which the foam can be secured with a little dab of glue. Most on-line vendors will only sell these fasteners in bulk amounts (>1000). Happily, a selection of these panel fasteners is available in smaller quantities from Non Ferrous Fastener, Inc.. Although the prototype shown to the right employs six single head ITWFastex clips received as a gift, the 1/4"×1.5" black clips which are sold

50/bag would appear to be equivalent (<http://www.non-ferrousfastener.com/products.php?cat=267&pg=2>). Plexiglas is brittle so that care must be taken while drilling the holes, otherwise it will chip or scratch. If one is available, a drill press operated at slow speed produces a very clean hole. Each sheet comes with a removable adhesive mask which was not taken off until drilling was completed. To ensure a proper match both sheets were taped together, drilled first with a small bit (1/8") after which the bit size was increased to match the final dimension recommended for the fastener. Following removal of the protective masking and thoroughly cleaning the Plexiglass components, the EL lamp was centered and then taped along the two long edges onto the black panel. Before fully assembling, holes (1.5" inches deep) were gently drilled into the foam using one of the Plexiglass sheets as a template. This greatly facilitated alignment of the foam with the posts exposed after the panel fasteners were pushed through the Plexiglass-ELP sandwich. A dollop of Barge all purpose cement was squeezed into each hole in the foam block and the posts carefully aligned before fully inserting them into the pre-formed holes. After turning the device foam-side up and making minor lateral adjustments to ensure the foam and Plexiglass-ELP sandwich were properly mated, the glued light-box was allowed to set overnight. The finished product, as seen from the bottom (Fig. 6) has been dubbed the "Lite ELPH" which is an acronym for



Lite-weight ElectroLuminescent Panel Housing.

Testing was performed to compare the output spectra and luminosity recorded using the split electrode and parallel electrode ELPs previously described. Since the A4 parallel electrode ELP is not large enough to fully illuminate either of my 8" catadioptrics (Celestron or Vixen), the 5" diameter cutout on the foam shroud was selected for use

Above (Fig. 5)
Face-up view of Plexiglass-ELP sandwich showing posts from 1.3" panel fasteners

Below (Fig. 6)
Bottom-side view of the Lite ELPH

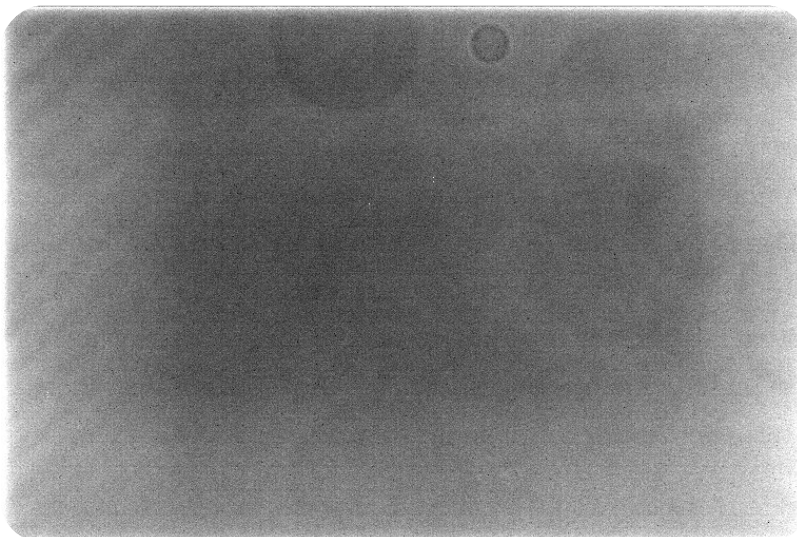


with a Televue NP101 refractor which nominally has 4" of aperture. As above, the same CCD camera (ST-402 ME) was used for flat fielding but this time in the comfort of my home office (Fig. 7). To thoroughly address whether the seam on the split-electrode lamp affects flat fielding, the following strategy suggested in part by Peter Kalajian from Alnatik Astrosystems (Sky and Telescope, March 2011) was employed. Twenty flats, dark-flats, and bias frames were taken after which the ELPH was rotated 90° and another series of 20 identical flats and dark flats were collected. All images were processed using the advanced calibration protocol in AIP4Win (v2.3.1). The first set was calibrated using the master flat (Fig. 8) generated from the second set of images and resulted in a highly uniform image consistent with excellent flat-field correction (Fig. 9). The resulting histogram (Fig. 10) was highly symmetrical (skew = 0.00431) and aside from three spurious pixels outside of 3σ deviations, the mean pixel value (11778.36) was within



Top right (Fig. 7)
Indoor Setup for Flat-fielding Televue NP101

Bottom (Fig. 8)
NP101 Master flat from average of 20 images

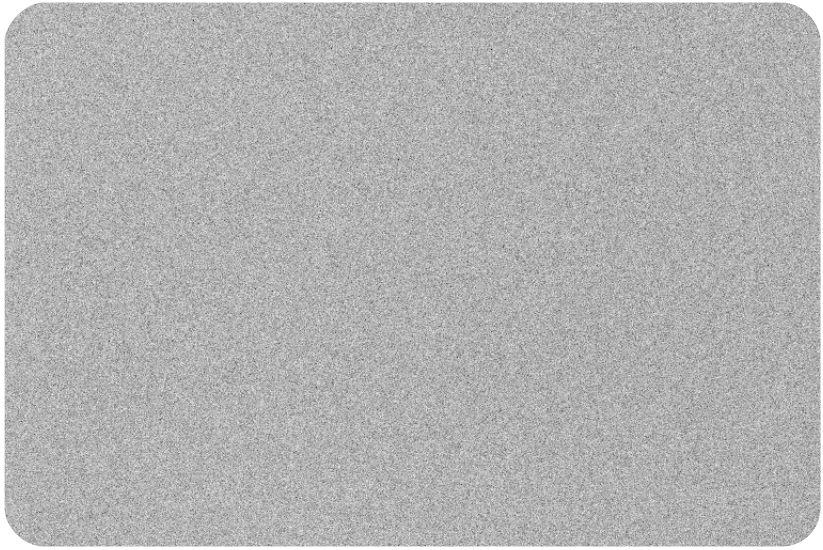


$\pm 0.468\%$. It would appear that since the seam in the split electrode lamp is so far out of focus, it is not detected in either flat. Flat fielding with the A4 parallel electrode revealed similar uniformity ($\pm 0.511\%$).

Narrow-band (<12 nm) filters presently used to image deep-sky objects are a testament to the improved sensitivity of digital cameras and increasing sophistication of today's amateur astrophotographer. The most common filters (H α , H β , OIII, NII, and SII) which are centered at 656.3, 486.1, 500.7, 658.4 and 672.4 nm, respectively, can be expected to greatly attenuate light output from the EL lamp. As can be seen in Figs. 12 and 13 this may be problematic for wavelengths longer than 650 nm (6500 Å). However, at least in the case of a Lumicon 48 mm H α Night Sky filter which is actually a cutoff filter (50% below 640 nm and transmission filter (90%) above 650 nm, there were

plenty of photons reaching the CCD camera. Unfortunately I do not have a bonafide narrow-band filter to test but expect that the exposure times will have to be significantly increased over those which typically work for standard RGB or photometric B, V, R and I_c filters.

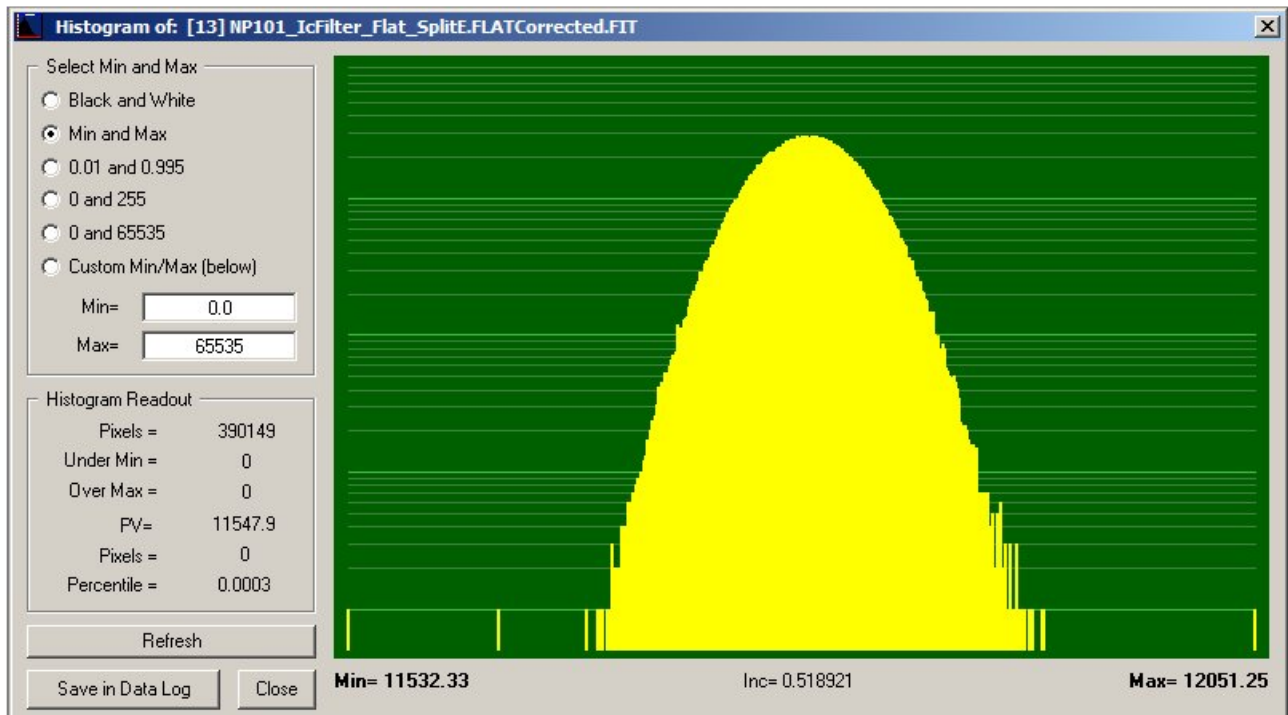
Despite the split-electrode lamp reference spectrum which was provided by the manufacturer (Fig. 2), I was not satisfied that the spectral output from the split- or parallel-electrodes had been adequately characterized under real-world conditions faced by the typical amateur astrophotographer. An SBIG Deep Sky Spectrograph (DSS 7) mated with the ST-402 ME camera proved to be invaluable for conducting a series of spectroscopic investigations. The DSS 7 is a moderate resolution (16 Å)

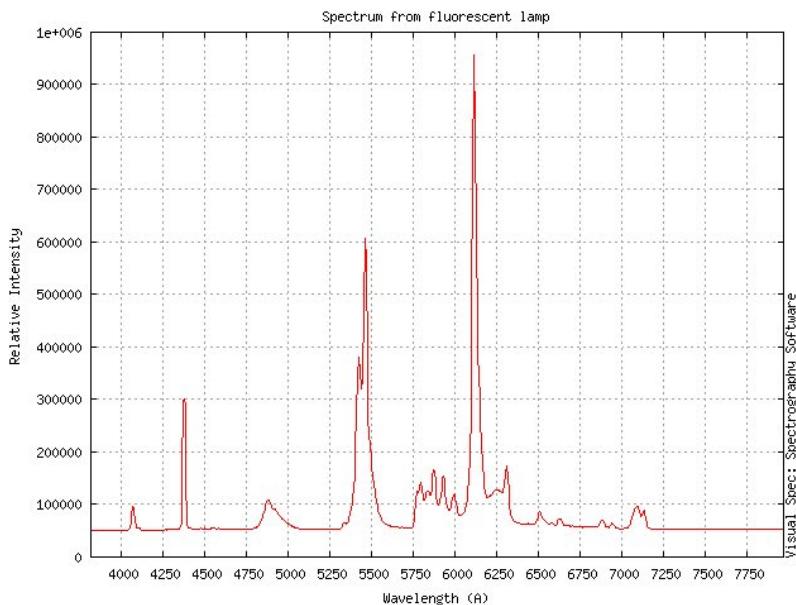


instrument designed to separate and focus wavelengths between 4000 and 8000 Å across the CCD array. A two point calibration (Visual Spec v3.8.8) was used to standardize spectra using the Hg (5465 Å) and Eu+3 (6116 Å) emission lines from a compact fluorescent lamp (Fig. 11).

Above (Fig. 9)
Flat-field corrected "flat" image after rotating position of ELPH by 90°

Below (Fig. 10)
Histogram from flat-fielded "flat" showing symmetrical distribution of pixel values from split-electrode lamp

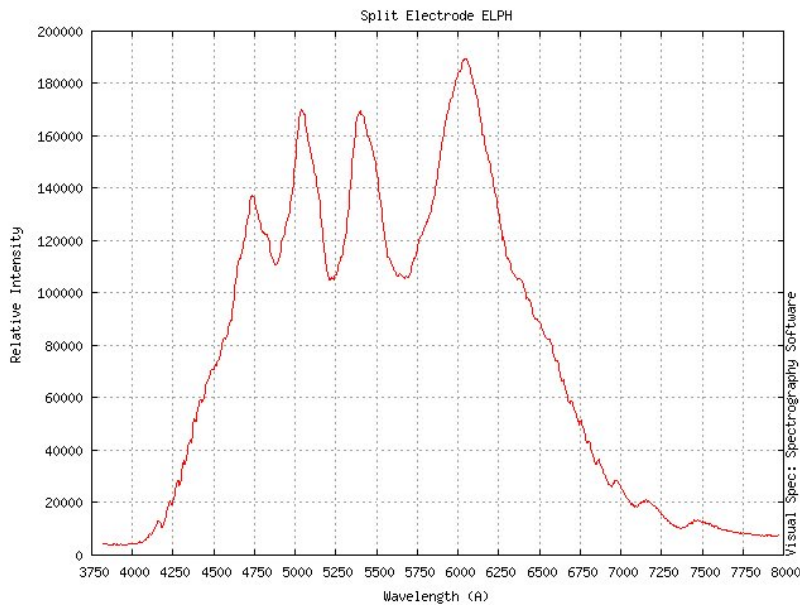




Above (Fig. 11)
Reference spectrum from compact fluorescent lamp

Below (Fig. 12)
Spectrum from split-electrode lamp

The results from the split-electrode and parallel-electrode ELPs are shown in Figs. 12 and 13, respectively. Significant differences between these two lamps were observed which in retrospect is not surprising since the chemical recipe each supplier uses for producing these panels is highly proprietary. The split-electrode spectrum (Fig. 1) provided by

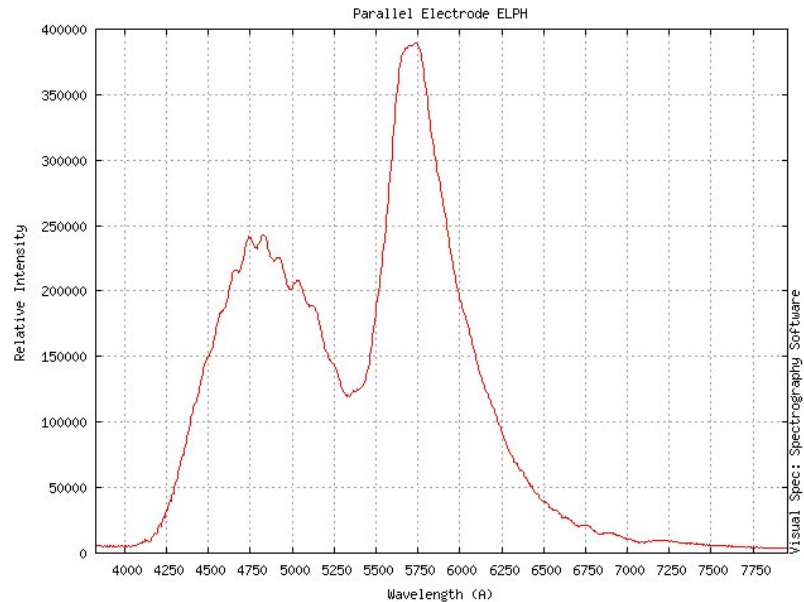


the manufacturer (<http://www.e-lite.com>) proved to be quite different possibly due to the higher operating voltage (280VAC) or major change in the lamp formulation since 1997 when the spectrum was taken.

In the same regard, the reader should also be cautioned that only one type of each ELP was tested making any conclusions about batch to batch uniformity or similar products from other suppliers impossible. Nonetheless, both panels produced plenty of flux for standard color and photometric filters in the blue (4000-5000 Å) and green (4750-5750 Å) wavelength regions. Exposure times for photometric B and V flats were less than 1.5 sec at the dimmest lamp setting. Even with the foam shroud, a white paper diffuser can be easily slipped in between the foam and working side of the lamp to further attenuate the output so that longer (>2 sec) exposure times are possible. As shown in Fig. 14, a single 8.5×11" sheet of Staples multipurpose paper (96 bright/20 lb) was tested using the DSS-7 spectrophotometer. There was ~50% reduction in total output but disproportionate losses were fairly obvious below 5500 Å. White Plexiglass did not exhibit this differential effect but appeared to reduce the signal equally across the measured wavelengths. Color and photometric R filters generally allow transmission in a range between 6000 and 7000 Å so that a CCD detector would also not suffer from lack of photons. Additionally, my guess is that flat fielding with narrow-band H β (4861 Å) or OIII (5007 Å) filters will

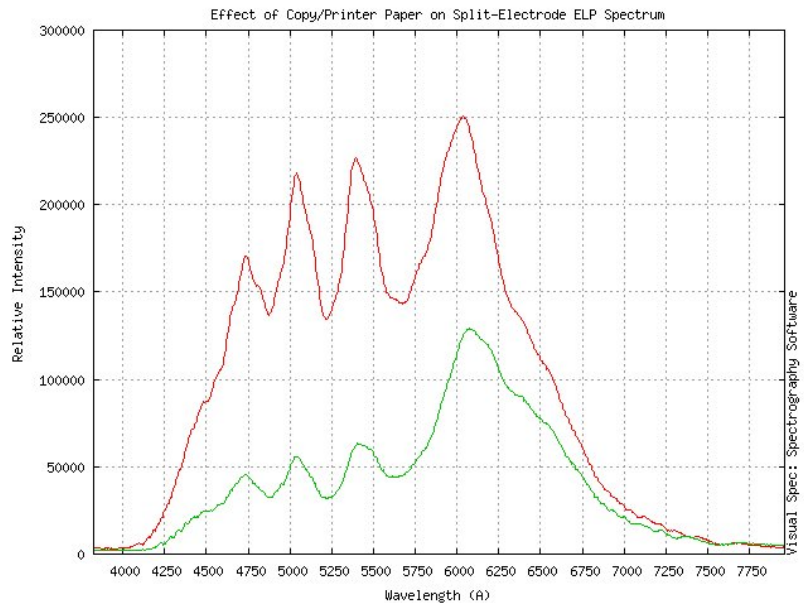
not require excessive exposure times. Above 6500 Å, however, the relative output of light from both lamps is low, particularly with the parallel electrode panel (Fig. 13). This is consistent with the longer exposure time (4 sec) at full intensity necessary to achieve 50% full well capacity with an I_c photometric filter. The practical importance of this dissimilarity suggests that much longer exposure times will be necessary to get flats from narrow-band H α (6563 Å), NII (6584 Å) and SII filters (6724 Å). All things considered for telescopes 8" and smaller, the 9"×12" split-electrode panel (pink off – white on) sourced from Knema, LLC is a good choice. The larger sized (A3 and A2) panels appear to be the parallel electrode type but were not tested during this assessment.

In summary, it is hoped that this article on the construction of a simple electroluminescent light box for flat-fielding will encourage others to do the same. Granted, I only looked at two of the many ELPs that are commercially available. The ready to use 9"×12" split-electrode EL panel is large enough to illuminate up to 8" of aperture and costs around \$160 including a dimmable inverter, power supply, two 12"×12"×1/8" Plexiglass sheets, and fasteners. Similarly, an A3 sized panel good up to 11" will set you back ~\$210 with dimmable inverter, power supply, two custom cut (16.75"×16.75" ×1/8") Plexiglass sheets and fasteners. Domestically (USA), cheaper alternatives may be



Above (Fig. 13)
Spectrum from parallel-electrode lamp

Below (Fig. 14)
Differential absorption of light (green curve) produced by the insertion of a white sheet of paper



found at the ElectroLuminescence, Inc. (http://e-luminates.com/osc3/product_info.php?cPath=27&products_id=93) or Glow Hut (<http://glowhut.com/el-strip--el-panel.html>) websites but they have a smaller selection of panel sizes and inverters. Irrespective of the vendor, this relatively modest expenditure in an era of multi-thousand dollar cameras,

mounts, and telescopes is arguably one of the best investments you can make if you are interested in simplifying the process of collecting flats and improving image quality. Don't hesitate to e-mail me through my observatory website (<http://www.underoakobservatory.com>) if you have any further questions.



Lunar image (3 sec exposure) taken with Nikon D70 through Televue NP101 at UnderOak Observatory. The starry field separately rendered is precisely superimposed onto the moon's location near mid-eclipse (3:20 am EST) on December 21, 2010.

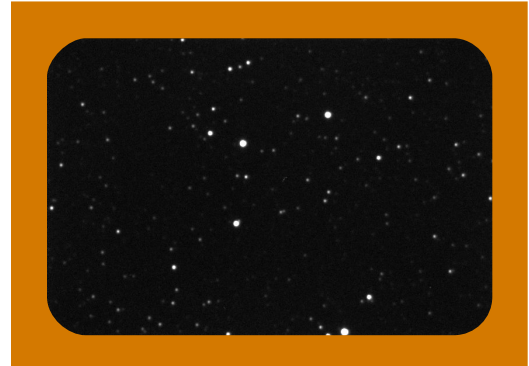
Photometry Basics

Part I: Detectors & Software

If you're ready to give pretty picture taking a rest consider joining the ranks of amateur astronomers who provide valuable support to the scientific community. In many cases you may already have all the equipment and software to begin collecting research quality photons. Over the next few issues of the "UnderOak Observer" I will share some of my experiences and hopefully point you in the right direction. Once again, please be reminded that I have absolutely no personal ties or financial interest in any of the vendors who are mentioned below.

Image acquisition, calibration and registration

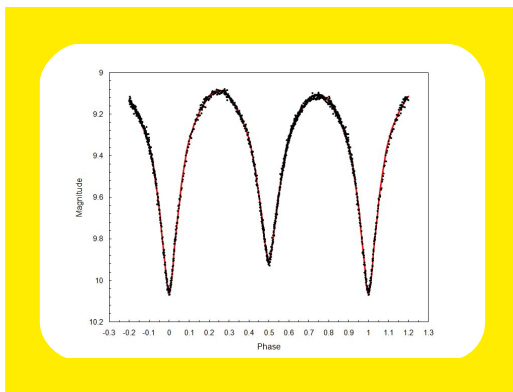
You can get your photometric feet wet using a DSLR, videocam, OSC or any monochromatic CCD camera with a clear filter to collect light curve data from a variable star. However, if you intend to share data with the scientific community, images captured in flexible image transport (fit) format with a monochromatic CCD camera through a B, V, R or I_c filter will be the most valuable. Two exceptions come to mind the first of which involves the study of minor planets. In this case, where the only objective is to determine the synodic period from a light curve then any digital camera with sufficient sensitivity will suffice. Similarly, light curve times-of-minimum for eclipsing binaries can be captured without regard to passband. My personal preference is the SBIG ST-402ME CCD camera (http://www.sbig.com/products/402_new.htm), a Peltier-cooled highly sensitive monochromatic detector accessorized with a photometric BVI_c filter wheel. This instrument has provided many years of trouble-free operation and is the perfect mate for SBIG's DSS-7 spectrograph.



Nowadays a sundry of commercial applications designed to automatically acquire and then calibrate and register images are available. CCDSoft has a long standing synergy with the SBIG line of CCD cameras and filter wheels and was the obvious choice six years ago when this investigator became serious about the study of minor planets and variable stars. Today there is a much longer list to pick from if you want to automatically control image acquisition; these include (but not necessarily limited to) MaxIm DL5, CCDAutoPilot 5.0, Nebulosity, AstroArt, and MPO Connections. How about image calibration and registration? Well, the choices grow even further and include CCDSoft5, AIP4Win, CCDStack, MaxIm DL5, Images Plus, MPO Canopus, Nebulosity, PixInsight, and AstroArt. For those on a tight budget applications such as IRIS and IRAF which are in the public domain may suit your needs. My personal choice for raw image calibration and registration is the very reasonably priced AIP4Win which by the way comes with a must-read monograph entitled "The Handbook of Astronomical Image Processing" by Richard Berry and James Burnell.

Photometric Reduction and Light Curves

Although many of the aforementioned commercial applications have photometry routines built in, MPO Canopus/PhotoRed stands alone at the top of the list with the most comprehensive set of tools to ease the tedium of converting specks of light on an image into a light curve. Brian D. Warner, an expert in minor planet photometry and inverse light curve modeling, is the brains behind MPO Canopus and its associated programs MPO Connections and MPO LCinvert. No less important, his companion book entitled "A Practical Guide to Lightcurve Photometry and Analysis" is a very readable treatise on this subject and comes highly recommended! The present price (\$65) for MPO Canopus is a steal considering the full range of capabilities offered in this application (<http://www.minorplanetobserver.com>).



Research Article

Photometric and Period Analysis of the Eclipsing Binary OO Aquilae

Abstract

OO Aql was targeted again at UnderOak Observatory since the first campaign in 2005 fell short of collecting a full set of light curves due to poor weather. Other important differences this time include photometric data collected in three bandpasses (B, V and I_C) as opposed to just a clear filter, period analysis of recent times-of-minimum data, and Roche modeling using a user friendly implementation of the Wilson-Devinney code (PHOEBE). Its brightness (V mag ~ 9.5), short orbital period (~ 0.5 d) and eclipse duration (~ 3 h) are amenable to investigation by amateur astronomers over a relatively short viewing campaign at locations with less than pristine seeing. Multi-color photometry has led to a revised linear ephemeris [Min. I (hel.) = 2455487.2995 + 0.5067933 E]. The updated O-C diagram continues to show sinusoidal-like short-term changes often attributed to magnetic activity cycles. All light curves (B, V and I_C) exhibit asymmetry at maximum light such that Max I is brighter than Max II. Roche modeling suggests the presence of a cool star-spot in the polar region of this binary system during the 2008 observation campaign.

1. Introduction

W UMa-type variable stars belong to a class of eclipsing binaries whose constituent main sequence stars (spectral type A–F to early K) are synchronized with respect to orbit and rotation. They rotate rapidly and are close enough that gravitational interaction has pulled them into a teardrop shape. An excellent summary of W UMa systems can be found at the AAVSO website (<http://www.aavso.org/files/vsots/wuma.pdf>).

OO Aquilae is considered an “overcontact” binary as both stars share a common envelope of material.

The variability of OO Aql was first reported by Dorrit Hoffleit (1932), a prodigious variable star investigator working in the observatories at Harvard and later, Yale University. Since then photoelectric or CCD derived light curves for OO Aql have been reported by a number of groups, including Binnendijk (1968), Lafta and Grainger (1985), Demircan and Gdr (1981), Essam et al. (1992), Gurol (1994), and more recently, Rucinski (1995), Djurašević and Erkačić (1999), Al-Naimiy and Al-Masharfeh (2000), Hrivnak et al. (2001) and Alton (2006). OO Aql consists of two main sequence stars (variously described between F8V and KoV) which are about the same mass but slightly more evolved than our Sun. More specifically, OO Aql belongs to the subclass of A-type W UMa binaries since the more massive ($M_1 = 1.06 M_{\text{Solar}}$) rather than less massive companion ($M_2 = 0.89 M_{\text{Solar}}$) is eclipsed at primary minimum. Typical of A-type W UMa systems, the temperature of the primary star is somewhat higher than the secondary. The orbital inclination angle is close to 86° so that our visual perspective of this system is nearly edge-on. This relatively bright variable is ideally suited for study as it is easily within the detection limits of a consumer grade digital camera coupled with a modestly sized telescope. OO Aql is less than 1° northwest of Altair and therefore suitably positioned for mid-latitude observers in the Northern Hemisphere during the summer and early fall seasons.

2. Observations and data reduction

2.1. Astrometry

Images of OO Aql were automatically matched against the standard star fields (UCAC3) provided in MPO Canopus (V10.3.0.2; Minor Planet Observer 2010).

This “automatch” feature generates a star chart centered on the putative center of the image and then matches the chart’s center, rotation, and scaling to the image. Plate constants are internally calculated which convert X/Y coordinates of a detected object to a corresponding RA and declination.

2.2. Photometry

CCD photometric measurements began on August 17, 2008 and finished 11 sessions later on September 24, 2008. Equipment included a 0.2-m Schmidt-Cassegrain telescope (f/6.3) with an SBIG ST-402ME CCD camera mounted at the primary focus. Automated multi-bandwidth imaging was performed with SBIG photometric B, V and I_C filters (<http://www.sbig.com/sbwhtmls/402bvi.htm>).

Typical image acquisition parameters, exposure (45 sec), and data reduction (lights, darks and flats) for this optical system have been described in detail (Alton 2009). Since accurate timings are critical, the computer clock was updated via the Internet Time Server immediately prior to each session. Image

acquisition (raw lights, darks, and flats) was performed using CCDSoft 5 while calibration and registration were accomplished with AIP₄Win (V2.3.1; Berry and Burnell 2008). Instrumental readings were reduced to catalog-based magnitudes using the MPOSC3 reference star fields built into MPO Canopus. No color or air mass corrections were applied.

2.3 Light Curve Analyses

Light curve modeling was performed using Binary Maker 3.0 (Bradstreet and Steelman 2002), PHOEBE (Prša and Zwitter 2005) and WDWint56a (Nelson 2009), all of which employ the Wilson-Devinney (W-D) code (Wilson and Devinney 1971; Wilson 1979). PHOEBE is a freely available (<http://phoebe.fiz.uni-lj.si/>) implementation of the W-D model which provides a user-friendly interface. Each model fit incorporated individual observations assigned an equal weight of 1. Spatial renderings of the modeled Roche geometry were produced by Binary Maker 3.0.

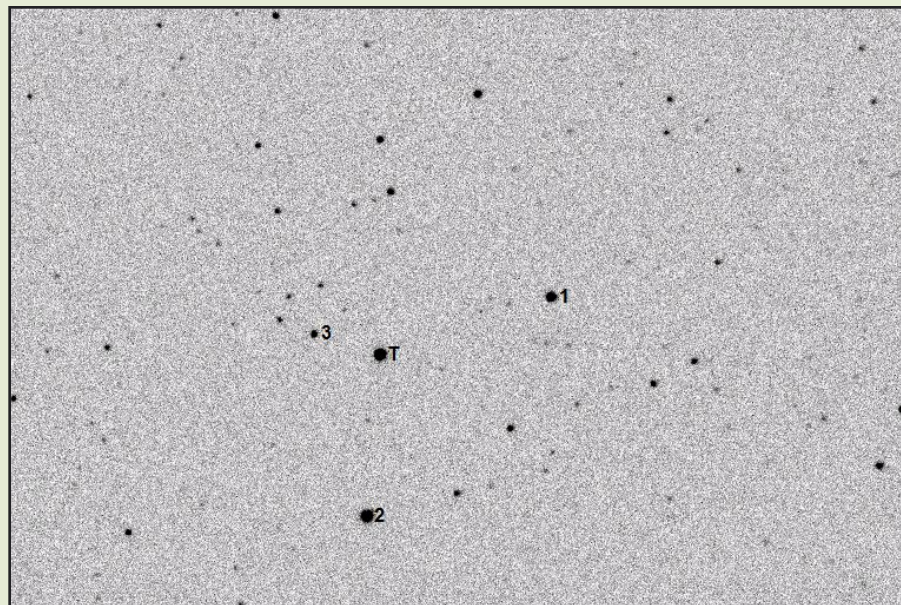


Figure 1.
Typical dark and flat field corrected CCD (B band) image of OO Aquilae (T) also showing the comparison stars (1-3).

3. Results and discussion

3.1. Photometry

OO Aql is located in the star-rich summer Milky Way so that finding comparison stars within the field of view (FOV \approx 10 \times 15 arc-min) captured by the optical system was not particularly challenging (Fig. 1). Three of the brightest stars (B mag) in the same FOV with OO Aql were selected to calculate the relative change in flux and derive catalog-based (MPOSC3) magnitudes using the “Comp Star Selector” feature in MPO Canopus. This hybrid derived-magnitude approach is accepted by the AAVSO for submitting CCD observations.

As is necessary with ensemble photometry, comparison stars cannot vary at least over the observation time span. This was verified prior to accepting data from each session; variability was generally within ± 0.03 mag for V and I_c filters and ± 0.05 for B passband. To minimize differential refraction and color extinction, only data at or above 30° altitude (airmass = 2.0) were used to produce light curves for OO Aql. Accordingly, airmass ranged from 1.18 to 1.86 during the entire 2008 campaign. Plotting the difference in magnitude over time from each comparison star against the averaged magnitude for all other comparisons yielded a narrow range of values with no obvious trend. A representative example is shown for a dataset (I_c filter) collected on August 17, 2008 (Fig. 2).

3.2. Ephemeris

Photometric values in B (n=1109), V (n=1163), and I_c (n=1179) passbands were combined by filter to produce light curves that spanned 5 weeks of imaging (Fig. 3). These observations included 21 new

times-of-minima (ToM) which were captured over seven nights. Initially seeded with the orbital period reported by Kreiner (2004), the Fourier analysis routine in MPO Canopus provided a period solution for the entire dataset. The time of minimum for the latest primary epoch was estimated using the Hertzprung method as detailed by Henden and Kaitchuck (1990); the corresponding linear ephemeris equation (1) was determined to be:

$$\text{Min. I (hel.)} = 2,454,695.6680 + 0.5068025 E \quad (1)$$

$$\pm 0.0000001$$

This orbital period captured over a relatively short time compares favorably with values reported over the past 5 decades. Independently, periodograms produced (Peranso v2.5, CBA Belgium Observatory) by applying periodic orthogonals (Schwarzenberg-Czerny 1996) to fit observations and analysis of variance (ANOVA) to evaluate fit quality confirmed

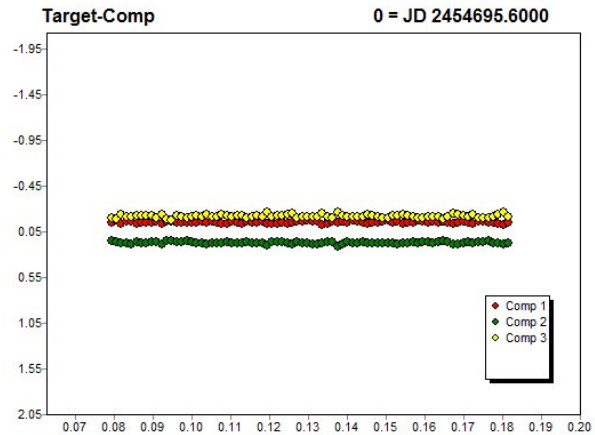


Figure 2. Typical differential magnitude (I_c) versus Julian Date for each of three comparison stars.

Star Identification	R.A.	DEC	MPOSC3 V mag	MPOSC3 B mag	MPOSC3 I _c mag
T. OO Aql	19:48:12.70	+09:18:32.3	(9.11–10.05) ^a	(9.85–10.85)	(8.34–9.22)
1. TYC 01058–0289 1	19:48:17.12	+09:21:17.7	10.487	11.683	9.842
2. TYC 01058–0409 1	19:48:01.91	+09:18:27.6	10.295	10.686	10.058
3. TYC 01058–0789 1	19:48:13.83	+09:17:26.5	11.876	13.189	11.170

a: Range of magnitudes for OO Aql from present study

Computed Time of Minimum (HJD-2400000.0)	ToM ±Error	UT Date of Observations	Type of Minimum
54695.6883	0.0002	17Aug2008	p
54703.5436	0.0003	25Aug2008	s
54704.5571	0.0004	26Aug2008	s
54705.5707	0.0007	27Aug2008	s
54710.6387	0.0003	01Sept2008	s
54724.5753	0.0004	15Sept2008	p
54725.5889	0.0002	16Sept2008	p

the period determination.

ToM values were estimated by MINIMA (V25b; Nelson 2007) using a simple mean from a suite of six different methods including parabolic fit, tracing paper, bisecting chords, Kwee and van Woerden (1956), Fourier fit, and sliding integrations (Ghedini 1981). Four new secondary (s) and three primary (p) minima were recorded during this investigation. Since no obvious color dependencies emerged, the timings from all three filters were averaged for each session (Table 2). These seven minima along with additional values published at the AAVSO, IBVS, VSOLJ and B.R.N.O. websites were used to update the OO Aql “Eclipsing Binary O–C” EXCEL spreadsheet file developed by Nelson (2005) and updated through 2005. The reference epoch from Kreiner (2004) was used to calculate O–C residuals and was defined by the following linear ephemeris equation (2):

$$\text{Min. I (hel.)} = 2,452,500.2635 + 0.5067926 E \quad (2)$$

$$\pm 0.0005 \quad \pm 0.0000002$$

Traditionally, an ephemeris (from the Greek ephemerios or “daily”), is a table which provides the location of an astronomical object at a particular time. The underlying mathematics used to predict the occurrence of an astronomical event can be very complex, however, the simplest equation ($y = c + a_1E$) is a straight line relationship anchored by a reference point in time (c), a constant multiplier (a_1) which is

the periodicity of the event and E , the cycle number. By convention with eclipsing binary star systems, time in an ephemeris equation is referenced relative to the primary minimum as seen from the Sun and is known as the Heliocentric Julian Date (HJD). This adjustment to the standard Julian date (which can be as much as ± 500 sec) provides a fixed reference point for all observations irrespective of calendar date. This is necessary since our position relative to the Sun is constantly changing as Earth moves around our home star.

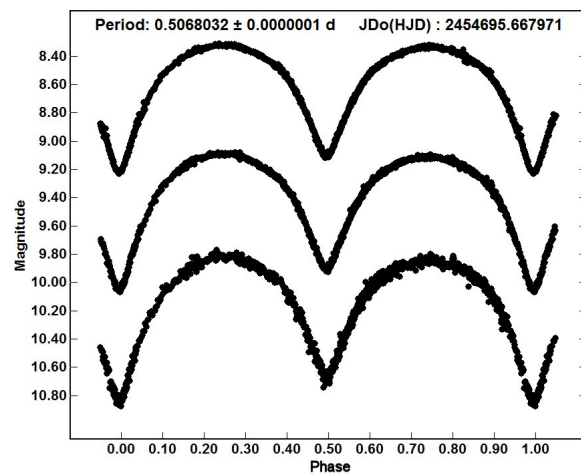


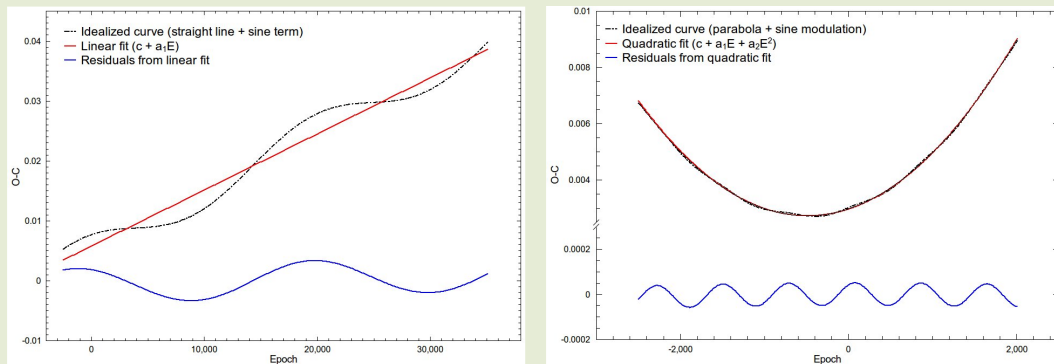
Figure 3. Folded CCD-derived light curves for OO Aql between Aug–Sept 2008. The top (I_C), middle (V) and bottom (B) curves shown above were analyzed using MPO Canopus and reduced to magnitudes from the MPOSC3 catalog.

O-C Method Primer

An in-depth discourse on the “O-C method” can be found in a book entitled “Introduction to Astronomical Photometry” by Budding and Demircan (2007) and is recommended reading for those interested in interpreting O-C diagrams. Both stars in a W UMa binary are tidally locked and therefore have circular orbits. The mathematics and interpretation of O-C data from systems with non-circular orbits observed with other types of eclipsing binaries is beyond the scope of this discussion. With this proviso in mind, if the O-C residuals versus time plot describes a straight line then the period being measured is constant. In this case $(O-C) = c + a_1E$ where a_1 is the period, c is the reference epoch and E is a relevant measure of time (HJD, cycle number, etc). Alternatively, an O-C diagram which produces a parabolic curve can be fit with a quadratic expression $(O-C) = c + a_1E + a_2E^2$. This relationship implies that the period is changing linearly with time. If a_2 , the coefficient of the quadratic term is greater than 0, then the period is increasing at a constant rate over time. An example of this behavior with the attendant formulae for calculating the rate (sec/year) of change is shown for AC Boo, another W UMa binary (Alton 2010). It follows that if $a_2 < 0$, then the apex of the parabola is pointing up instead of down and the period is decreasing in a linear fashion. In many cases, a linear change in orbital period is attributed to either mass exchange between the primary and secondary constituents or some mechanism which results in angular momentum loss from the binary system. The last remaining predictable relationship between residuals and time that is commonly observed in O-C plots produces a cyclical pattern. This kind of modulation can be macroscopically obvious or may need to be teased out using regression techniques. If the underlying behavior is sinusoidal, this variation can be fit to an expression which takes the general form:

$$O-C = c + a_1 \cdot E + a_2 \cdot E^2 + a_3 \cdot \sin(a_4 \cdot E + a_5)$$

where a_3 is the amplitude of the period oscillation, a_4 is the oscillation period and a_5 is an offset factor necessary to phase the data. The idealized plot shown below (left side) is a simulation of obvious sinusoidal behavior suggestive of long-term periodicity whereas the right-side figure is more in line with shorter term low amplitude periodicity that needs to be teased out using regression analysis.



In reality, not all O-C plots will fit into the tidy categories described above. There are also cases where the data points can be approximated by a high-order polynomial or exhibit a step-wise appearance such that period changes are abrupt or occur in an irregular sequence. Each O-C diagram produces a unique fingerprint of binary activity which will require varying levels of detective work to build a hypothesis about what mechanism(s) are responsible for changes in periodicity.

All of the O-C diagrams herein were produced using QtiPlot (v0.9.8 2010), an open source application running on Ubuntu Linux. A demo version is also available for PC and Mac users; fully operational versions can be purchased for a modest price (<http://soft.proindependent.com/qtiplot.html>).

A comprehensive set of “observed minus calculated” (O-C) data from 1932 through 2010 is reproduced herein (Fig. 4). Over the course of time (which can be many decades for well-studied systems), O-C diagrams from most W UMa binary systems rarely exhibit only a simple straight-line relationship. In contrast, what is usually seen is a complex mixture of parabolic, sinusoidal and/or linear segments which provide a fingerprint for period changes experienced by each binary system. The O-C diagram for OO Aql is obviously not going to set a new standard for simplicity. The first noteworthy pattern is that O-C variability decreased significantly after cycle 2000 and is largely due to the preponderance of photometrically-derived rather than visual data. Therefore, for calculation purposes, CCD and photoelectric observations were weighted 8-fold while visual and photographic times-of-minima were assigned a value of 1. Regression analyses using a scaled Levenberg-Marquardt algorithm was performed with QtiPlot (v0.9.8 2010), an open source application running on Ubuntu Linux. A fifth-order polynomial was the lowest order expression that produced a good fit ($r^2 > 0.97$) of all the data. Borkovits et al. (2005) proposed the existence two fundamental periods which included the first harmonic for a long-period (~ 75 yr) sinusoidal change as well as one for short period (~ 20.25 yr) fluctuations. The most obvious visual cue to the long-period is the two major nodes observed around cycles -30732 (Dec1959) and -2167 (Aug1999). A “back-of-the-envelope” estimation shows that these are separated by ~ 39.6 years. Projecting out one full cycle yields 79.3 years, which is slightly longer than that calculated by Borkovits et al (2005) but less than that proposed (89 yr) by Demircan and Gürol (1996). Nonetheless, since only a single long term cycle has barely been completed by any estimate, we’ll probably have to wait beyond ~ 2038 before the next node is obvious according to these predictions. If truly sinusoidal, this long period change is consistent with a light time effect from an unseen companion. Lafta and Grainger (1985) had suggested that period fluctuations may result from a third body or nodal

regression and more recently, additional support for a very close companion using adaptive optics is described by Rucinski et al (2007).

The short-term cyclic changes described by Borkovits et al (2005) are less obvious due to variability in the O-C curve. Residuals from the fifth-order polynomial fit (Fig. 5) revealed that the $(O-C)_2$ data could be modeled by a quadratic expression modulated with a sinusoidal term as follows:

$$O-C = 0.003199 (\pm 0.0002) + 1.463 (\pm 0.276) \times 10^{-7} \cdot E + 2.27 (\pm 0.77) \times 10^{-12} \cdot E^2 + 3.44 (\pm 0.22) \times 10^{-3} \cdot \sin [4.068 (\pm 0.049) \times 10^{-4} \cdot E + 7.829 (\pm 0.703)] \quad (3)$$

The amplitude (0.00344 day) of the periodic oscillation is defined by the coefficient of the sine term. According to the relationship:

$$P_3 = 2\pi P / \omega, \text{ where } \omega = 4.068 \times 10^{-4} \quad (4)$$

the cyclic period would be ~ 21.4 years and nearly identical to that predicted by Borkovits et al (2006). These short-term modulations (18-20 years) commonly observed in other W UMa binary systems are attributed to changes in magnetic activity, not unlike the sun-spot cycle experienced by our host star. This phenomenon first formalized by Applegate (1992) proposes that a change in the gravitational quadrupole moment of an active binary star can modify the orbital period within decades rather than millennia. Furthermore, the “Applegate effect” posits that orbital angular momentum remains constant so that when the quadrupole moment increases by some mechanism, the gravitational pull on the companion star increases bringing them closer together with an attendant increase in the orbital period. In a similar fashion, should the quadrupole moment decrease, the orbital period also decreases as the stars move farther apart.

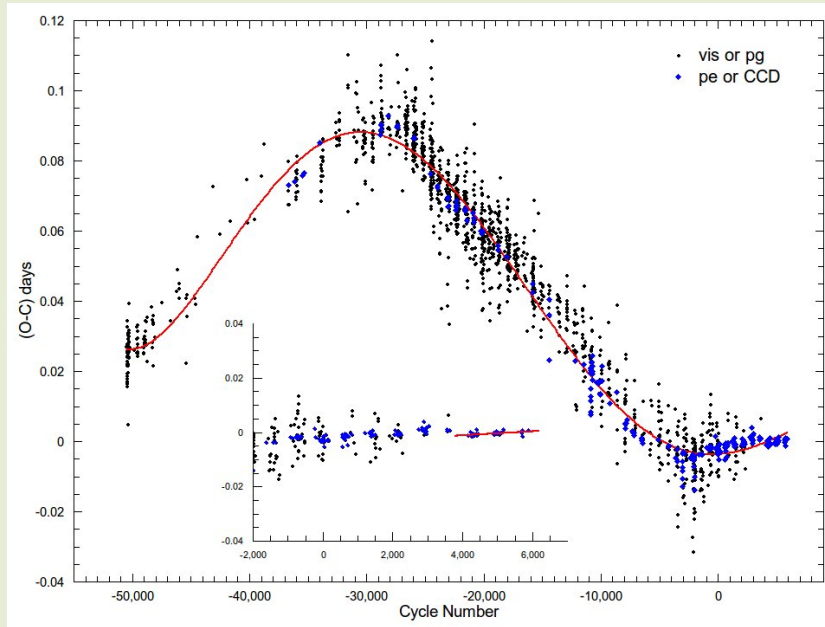


Figure 4. O-C diagram for OO Aql comprised of visual, photographic, photoelectric and CCD observations collected by various investigators since 1932. Two major inflection points are seen around cycles -30732 (Dec1959) and -2167 (Aug1999). Inset figure shows straight-line segment used to determine linear ephemeris from near term timings (May 2008 – October 2010).

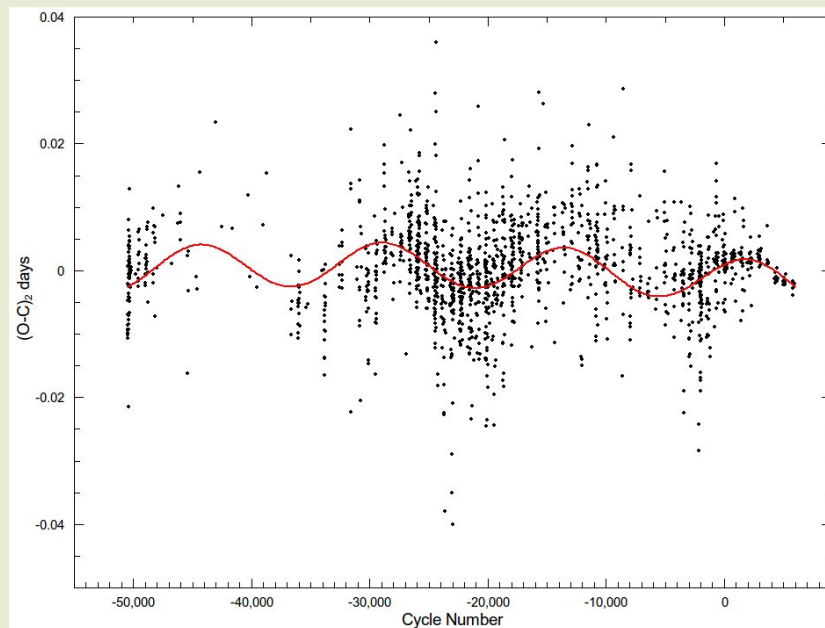


Figure 5. Plot of 5th-order polynomial residuals versus cycle number showing short-term (~21 yr) cyclical changes since 1932. The nonlinear quadratic+sine term fit of the $(O-C)_2$ residuals vs cycle number is shown in red.

As had been mentioned previously a linear ephemeris equation is based on the assumption that the primary minimum had or will occur at some whole number multiple (cycle number) of a fixed periodicity starting at a reference point in time. It goes without saying that since the orbital period of OO Aql simultaneously experiences long-term (75-89 yr) and short-term (~ 21.4 yr) changes there cannot be a single linear ephemeris equation which can predict accurately when Min I will occur in the distant future. Visual inspection of the inset plot in Fig. 4 reveals that a straight-line segment can be drawn starting at cycle 4137 and continuing to the last data point. A revised linear ephemeris equation (3) was therefore calculated based upon these near term O-C data:

$$\text{Min. I (hel.)} = 2455487.2995 + 0.5067933 E \quad (5) \\ \pm 0.0008 \pm 0.0000002$$

As such, should the complex O-C behavior of this system continue unabated, revised ephemerides for OO Aql will need to be calculated on a regular basis.

3.3 Light Curve Synthesis

Individual light curves comprised of all observations irrespective of bandpass (Fig. 3) show that minima are separated by 0.5 phase which is a prerequisite for a circular orbit. It is theoretically possible, however, from certain vantage points to observe minima separated by 0.5 phase from binaries with elliptical orbits, however, it is highly unlikely that this would occur in contact systems which are tidally locked. Also noteworthy is the asymmetry in maximum light ($\text{Max I} > \text{Max II}$) which is clearly seen in all colors. In addition, all three filters produce unequal depths at minimum light ($\text{Min I} < \text{Min II}$). With the exception of the 1987 light curves (B and V) reported by Essam et al (1992) in which $\text{Max I} < \text{Max II}$, all others show maximum light with varying differences following primary minimum (Binnendijk (1968), Lafta and Grainger (1985), Demircan and Gdr (1981), Grol (1994), Djuraevi and Erkapi (1999), Rucinski (1995), Hrivnak et al. (2001) and the present paper). A

plausible explanation for this variability is attributed to the so-called O'Connell effect and may involve the presence of starspot(s) on one or more binary components. An excellent review of the O'Connell effect in eclipsing binary systems can be found in a publication by Wilsey and Beaky (2009). Within that paper a number of theoretical models which could explain the diagnostic out-of-eclipse asymmetry at maximum light are discussed. The most thoroughly documented approach to model this effect has been to invoke the presence of starspot(s). Analogous to differential rotation on the Sun, localized magnetic disturbances on W UMa binaries can block convective motion towards the surface and result in cool starspots which may survive for a protracted period of time (Berdyugina 2005). Alternatively, hot spots akin to solar flares may also appear but usually evolve quickly. Both phenomena disrupt luminous homogeneity and can produce asymmetric features on a light curve. The Roche model derived from the seminal Wilson and Devinney (1971) paper has been widely used to provide synthetic light curve solutions which closely fit changes in flux arising from eclipsing binary star systems. The corresponding W-D computer code has evolved to accommodate the introduction of idealized circular starspots to improve the model fit. At this time no software routine within the W-D code has been implemented for any of the alternative theories which might account for light curve asymmetry. It is likely this limitation which fails to address other sources of light curve variability has led to the overuse of starspot modeling. Nonetheless, at this time no other theory has accumulated sufficient experimental evidence to completely displace the presence of starspot(s) as a more viable explanation for the O'Connell effect.

Mode 3 (overcontact binary but not in thermal contact), synchronous rotation and circular orbits were chosen to begin Roche modeling by PHOEBE. Bolometric albedo ($A_{1,2}=0.5$) and gravity darkening coefficients ($g_{1,2}=0.32$) for cooler stars with convective envelopes were assigned as reported by Rucinski (1969) and Lucy (1967), respectively. After

any change in T_{eff} , logarithmic limb darkening coefficients (x_1 , x_2 , y_1 , y_2) for both stars were interpolated within PHOEBE according to Van Hamme (1993). OO Aql conforms to the A-subtype where the most massive and hotter star is eclipsed at primary minimum. The smaller secondary star has the lowest surface temperature, and contributes less to the overall luminosity of this binary system. The effective temperature (T_{eff}) of the primary can be estimated from first principles as follows from the B-V magnitude determined during Min II when the primary occults the secondary and its spectral output is least contaminated. Since W UMa systems are invariably comprised of main sequence (dwarf) stars, the mean B-V value (0.76) corresponds to an effective temperature of 5386 °K (Flower 1996) which is somewhat cooler than our sun (~5800 °K). However, recalling that this star system resides in a dust-rich region of the summer Milky Way, a correction has to be made to account for interstellar reddening, which results from disproportionately high absorption and scattering of blue light by interstellar dust. In the UBV photometric system this adjustment factor $E(B-V)$ also known as color excess is related to the observed and intrinsic B-V value in the following manner:

$$\begin{aligned} E(B-V) &= (B-V)_{\text{observed}} - (B-V)_{\text{intrinsic}} \text{ or} \\ (B-V)_{\text{intrinsic}} &= (B-V)_{\text{observed}} - E(B-V) \end{aligned} \quad (6)$$

There are multiple lines of evidence from other investigations that suggest the spectral type of OO Aql ranges between F8V and KoV (Eggen 1967, Rucinski & Kaluzny 1981, and Pribulla et al 2007). The SIMBAD astronomical database (<http://simbad.ustrasbg.fr/simbad/>) along with a recent compendium of W UMa binaries (Awadalla and Hanna 2005) lists OO Aql as G5V which is essentially half-way between F8V and KoV. Estimates for galactic dust reddening and extinction can be mined from the NASA/IPAC Infrared Science Archive (<http://irsa.ipac.caltech.edu/applications/DUST/>). The $E(B-V)$ value in the region (5 arcmin radius) around OO Aql averages 0.2613; therefore according to Equation 6, $(B-V)_{\text{intrinsic}}$ is equal to 0.499 and

corresponds to an F8V star which is quite a bit hotter (6282 °K). According to Pribulla et al (2007) the mass of the primary (1.058) is more in line with a G1V star. Overall, the latest scorecard for the spectral classification of this binary system seems to favor a primary which ranges between F8V and G2V. T_{eff} for the primary (T_1) was set equal to 5943 °K based on tabulated values (de Jager and Nieuwenhuijzen 1987) for a GoV main sequence star, the mid-point between F8V and G2V. For modeling purposes, the effective temperature of the secondary (T_2) was assigned a starting value of 5890 °K based upon the ΔT ($T_1 - T_2 \approx 50$ K°) generally reported by others (Hrivnak et al 2001, Awadalla & Hanna 2005, and Djurašević & Erkačić 1999). Parenthetically, a mid- to high-resolution spectrum of OO Aql taken during Min II could be very helpful in nailing down the spectral classification of the primary star.

3.4 Roche Modeling

The most recent value for the mass ratio ($M_2/M_1 = q_{\text{sp}}$) was derived from radial velocity experiments, the gold-standard for such measurements (Pribulla et al 2007). This value (0.846) and those for $\Omega_{1,2}$ (3.39) and i (87.7°) reported by Hrivnak et al (2001) were used as a starting point for an unspotted fit using the commercial application Binary Maker 3 (BM3). This Java-based program has proven to be an invaluable tool for roughing out a model fit prior to further refinement using PHOEBE or WDWint. Initial attempts involved iteratively adjusting the effective temperature of the secondary (T_2), orbital inclination (i), limb-darkening (x_1 and x_2 ; linear-cosine) and common envelope surface potential ($\Omega_1 = \Omega_2$) until a reasonable fit of the model to phase normalized flux (V band) was obtained. In contrast to BM3, model fitting in PHOEBE employed phased data which had been converted into catalog-based magnitudes. A_1 , A_2 , g_1 , g_2 , q , and T_1 were fixed parameters whereas $\Omega_{1,2}$, T_2 , phase shift, luminosity, x_1 , x_2 , y_1 , y_2 , and i were iteratively adjusted while using differential corrections (DC) to achieve a simultaneous minimum residual fit of all (B, V, and I_c) photometric

observations. Starting with a no-spot model in PHOEBE, the initial values from BM3 quickly converged to a new solution which very adequately fit Max I but over-estimated Max II (Fig. 6). One of the challenges with invoking a star-spot model is deciding how to deal with the large number of possible solutions. If the target being studied has prior history, then this can be an important guide to predicting whether a cold spot is more likely than a hot spot or whether the primary as opposed to the secondary star is affected. As had been previously mentioned, aside from the light curves generated by

Essam et al. (1992), maximum light followed the primary minimum in all others. In keeping with the K.I.S.S. principle, two possible solutions can be proposed based on the following considerations. Is the maximum (Max I) following primary minimum higher than it would be without any starspot, or is Max II lower than it would be under the same circumstances? Since the Lafta and Grainger (1985) light curves analyzed by Djurašević & Erkačić (1999) were also brighter during Max I, their model fit using a cool spot on the primary seemed to be a reasonable starting point. Unlike Djurašević & Erkačić (1999)

Table 3. A Comparison of Selected Geometrical and Physical Elements for 00 Aquilae Obtained Following Roche Model Light Curve Fitting			
Parameter	Present Study		Djurašević & Erkačić 1999 ^d Cold Spot on M ₁
	Cold Spot on M ₁	Cold Spot on M ₂	
T ₁ (°K) ^b	5943	5943	5700
T ₂ (°K)	5813 (1)	5808 (1)	5638±6
q (M ₂ /M ₁) ^b	0.846	0.846	0.843
A ^b	0.5	0.5	0.5
g ^b	0.32	0.32	0.32
Ω ₁ = Ω ₂	3.431 (0.002)	3.423 (0.002)	3.46
i°	85.99 (0.08)	86.36 (0.07)	86.1±0.2
A _s = T _s /T	0.807 (0.004)	0.851 (0.006)	0.67
Θ _s (spot co-latitude)	15°	40°	16.1°
φ _s (spot longitude)	35°	240°	93.2°
r _s (angular radius)	32.18° (0.12)	21° (0.18)	38.9°±0.4
r ₁ (back)	0.4353	0.4370	0.4272
r ₁ (side)	0.4006	0.4018	0.3949
r ₁ (pole)	0.3790	0.3799	0.3745
r ₁ (point)	0.5172	0.5172	0.5176
r ₂ (back)	0.4061	0.4078	0.3970
r ₂ (side)	0.3697	0.3708	0.3634
r ₂ (pole)	0.3512	0.3521	0.3460
r ₂ (point)	0.4828	0.4828	0.4824
χ ² (B) ^c	1.497	1.493	-
χ ² (V)	1.064	1.069	-
χ ² (I _c)	3.367	3.406	-
Σ(0-C) ² ^e	0.01061	0.00963	0.01557

a: Error estimates in parentheses from WDWint56a (Nelson 2009)
 b: Fixed elements during DC
 c: χ² from PHOEBE (Prša and Zwitter 2005)
 d: V mag only; r₁ and r₂ estimated using Binary Maker 3
 e: Σ(0-C)² sum of squares of residuals between observed and synthetic curves

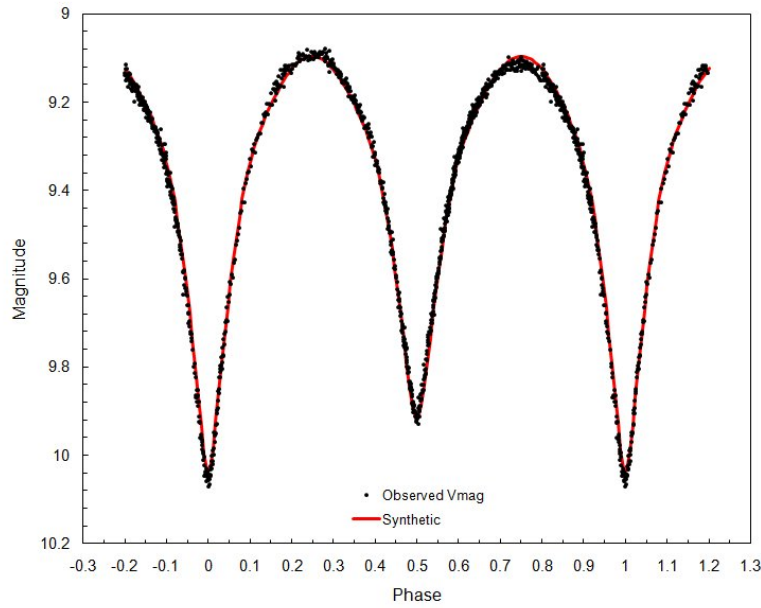


Figure 6. Unspotted Roche model fit of V mag light curve for OO Aql (2008). Synthesized curve slightly over-shoots maximum light at Max II

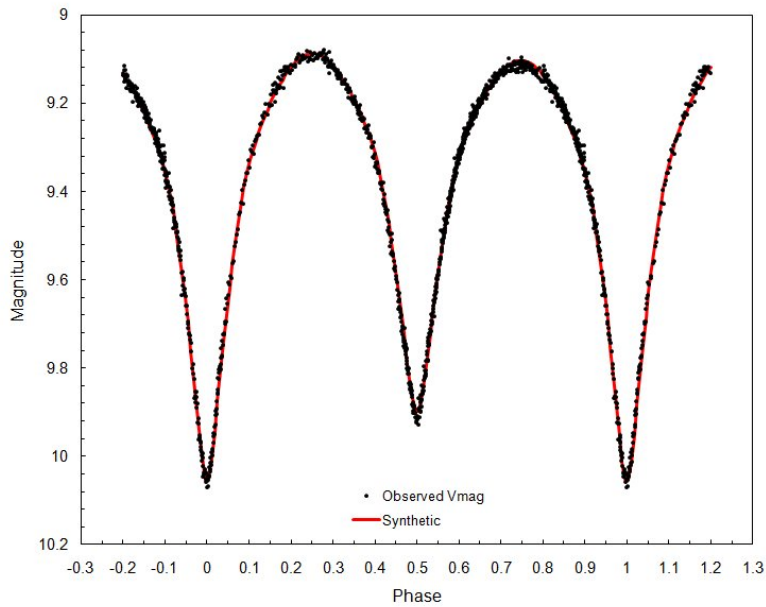


Figure 7. Roche model fit of V mag light curve for OO Aql (2008) with cool spot positioned in the polar region of the primary star.

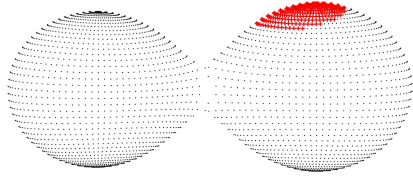


Figure 8.
Roche model 3-D rendering of OO Aql showing position of cool spot on primary star.

who separately modeled each bandpass (B and V), the present work takes a more rigorous approach by simultaneously achieving a model fit in all three colors (B,V and I_c). This is in no way intended as a criticism, but rather speaks to the powerful W-D code (WDWint and PHOEBE) now in the public domain which facilitates this process. Elements for OO Aql obtained with a cold spot on the primary star using PHOEBE are provided in Table 3; absolute system parameters based upon the radial velocity findings of Pribulla et al (2007) are provided in Table 4. A representative light curve (V mag) with the associated synthetic fit and a geometric rendering produced with BinaryMaker 3 are illustrated in Figs. 7 and 8, respectively. Whilst the model fit appears to be quite satisfactory, the solution is not unique. Although no simple combination of hot spots on either binary could reproduce the asymmetry observed at maximum

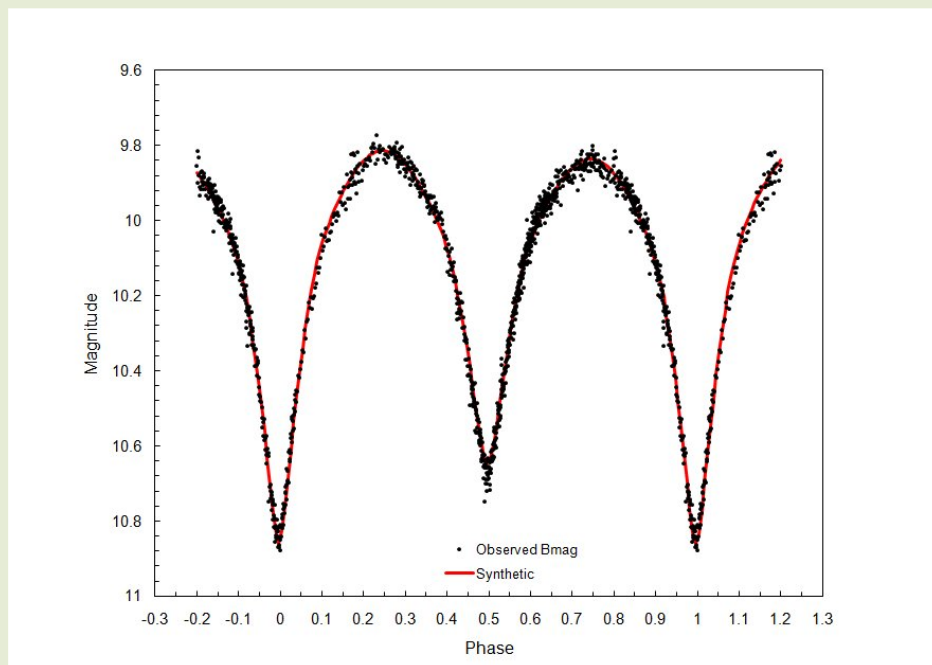


Figure 9.
Roche model fit of B mag light curve for OO Aql (2008) with cool spot positioned in the polar region of the secondary star.

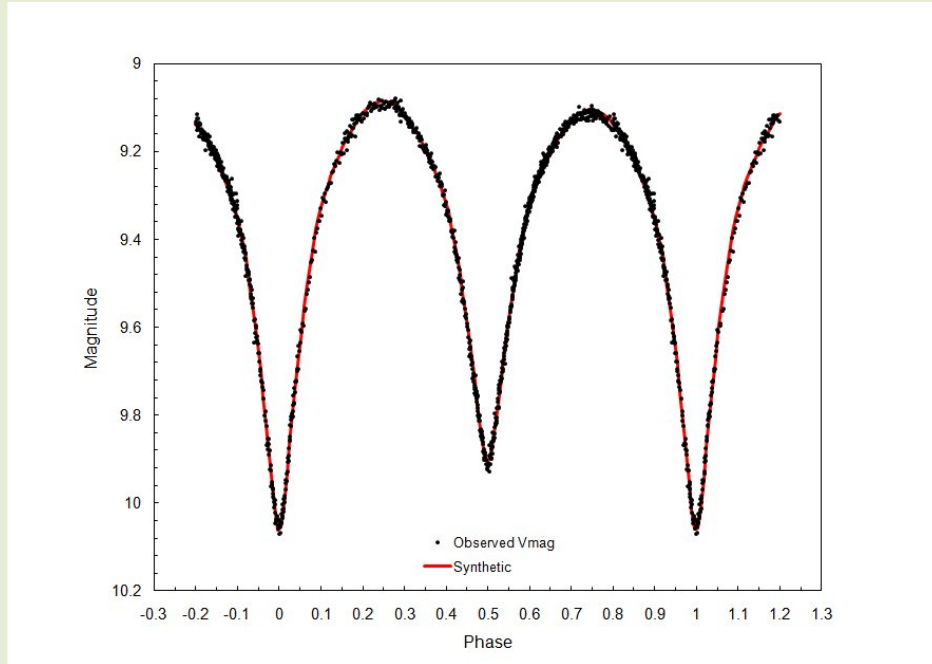


Figure 10.
Roche model fit of V mag light curve for OO Aql (2008) with cool spot positioned in the polar region of the secondary star.

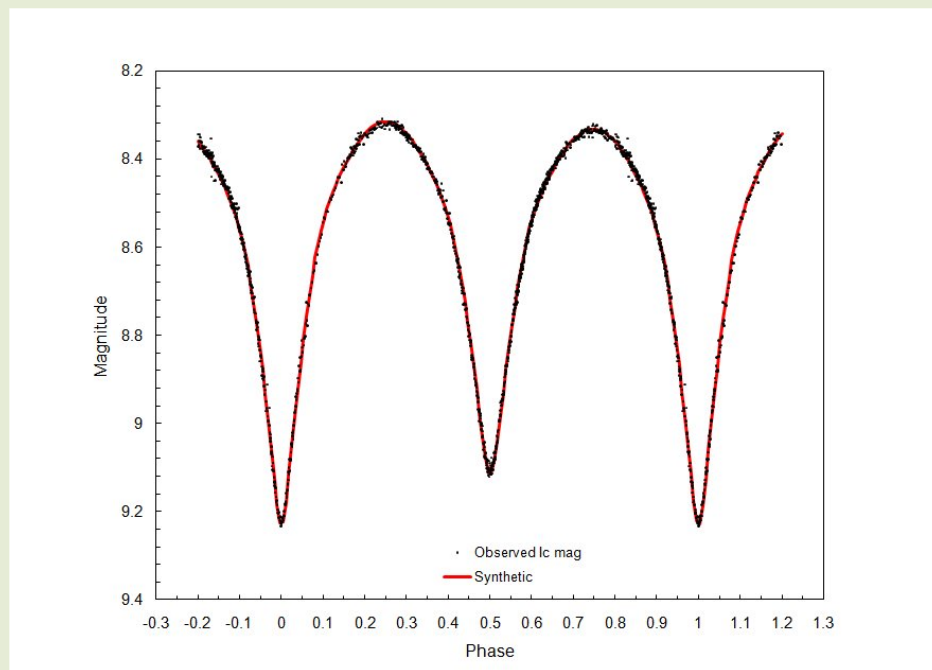


Figure 11.
Roche model fit of I_c mag light curve for OO Aql (2008) with cool spot positioned in the polar region of the secondary star.

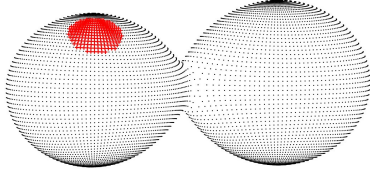


Figure 12.
Roche model 3-D rendering of OO Aql showing position of cool spot on secondary star.

light with this dataset, placement of a cool spot on the secondary star resulted in a marginally better fit (Table 3). These latter light curve fits are reproduced in Figs. 9 (B mag), 10 (V mag), and 11 (I_c mag); a 3-dimensional spacial model for OO Aql showing the cool spot located on the secondary is shown in Fig. 12. The positioning of a spot in the polar region is common to both cool spot solutions and highlights the challenge that often arises in trying to find an unambiguous fit to light curve data. Despite the slightly improved overall goodness of fit ($\Sigma(O-C)^2$) achieved with a cool spot on the secondary, it would be presumptuous to pick one spot model fit over the other.

4. Conclusions

CCD photometric readings in B, V and I_c passbands have led to the construction of light curves which have been used to revise the linear ephemeris [Min. I (hel.) = 2455487.2995 + 0.5067933 E] for OO Aql. The updated O-C diagram continues to show sinusoidal-like short-term changes (~ 20 yr) often attributed to magnetic activity cycles. As has been primarily observed by other investigators, the 2008 light curves exhibit asymmetry at maximum light such that Max I is brighter than Max II. Roche modeling suggests the presence of a cool spot in the polar region(s) of this binary system, however, its physical assignment to a specific star was not possible since the goodness of fit was not meaningfully different with a cool spot positioned on either component. Arguably, however, it is entirely possible that an unrelated mechanism is involved in perturbing the light curve for this binary system.

Public access to any light curve data associated with this research can be obtained by making a written request to mail@underoakobservatory.com

5. Acknowledgements

This research has made use of the SIMBAD database, operated at Centre de Données astronomiques de Strasbourg, France. Time-of-minima data from the B.R.N.O., IBVS, AASVO, and VSOLJ websites proved

Parameter	Present Study	
	Cold Spot on M_1	Cold Spot on M_2
$M_1(M_\odot)$	1.058 ^a	1.058 ^a
$M_2(M_\odot)$	0.895 ^a	0.895 ^a
$R_1(R_\odot)$	1.374	1.364
$R_2(R_\odot)$	1.276	1.267
$\log(g)_1$	4.186	4.192
$\log(g)_2$	4.177	4.184
$a(R_\odot)$	3.34	3.34
f(% overcontact)	13.63	15.33
a: Pribulla <i>et al</i> 2007		

invaluable to the assessment of period changes experienced by this W UMa variable over the past 8 decades. The diligence and dedication shown by all associated with these organizations is very much appreciated. In addition, the SAO/NASA Astrophysics Data System (http://adsabs.harvard.edu/abstract_service.html) was extensively used to conduct literature searches in support of this study.

6. References

- Al-Naimiy, H.M.K. and Al-Masharfeh, T.H.SH. 2000, *Astrophysics and Space Science*, 273, 83.
- Alton, K. 2006, *JAAVSO*, 34, 1.
- Alton, K. 2009, *JAAVSO*, 37, 148.
- Alton, K. 2010, *JAAVSO*, 38, 57.
- Applegate, J.H. 1992, *ApJ* 385, 621.
- Awadalla, N.S. and Hanna, M.A. 2005, *J. Korean Astron. Society*, 38, 43.
- Berdyugina, S.V. 2005, *Living Reviews in Solar Physics*, 2, 8.
- Berry, R., and Burnell, J. 2005, *Handbook of Astronomical Image Processing*, Willmann-Bell, Richmond.
- Binnendijk, L. 1968, *Astrophys. J.*, 73, 32.
- Borkovits, T., Elkhateeb, M. M., Csizmadia, Sz., Nuspl, J., Biró, I. B., Hegedüs, T., and Csorvási, R. 2005, *Astron. Astrophys.*, 441, 1087.
- Borkovits, L., Csizmadia, Sz., Nuspl, J. and Biró, I. B. 2006, *PADEU*, 17, 109.
- Bradstreet, D.H. and Steelman D.P. 2002, *Bull. A.A.S.*, 34, 1224.
- Cox, A.N. 2000, *Allen's Astrophysical Quantities*, Springer-Verlag New York, Inc.
- Demircan, O., and Güdür, N. 1981, in *Photometric and Spectroscopic Binary Systems*, ed. E. B. Carling and Z. Kopal, Reidel, Dordrecht, 413.
- Djurašević, G., and Erkačić, S. 1999, *Astrophys. Space Sci.*, 262, 305.
- Eggen, O.J. 1967, *Mem. R. astr. Soc.*, 70, 111.
- Essam, A., El-Bassuni, A.A., and Mahdy, H.A. 1992, *Astrophys. Space Sci.*, 188, 127.
- Flower, P.J. 1996, *Astrophys. J.*, 469, 355.
- Ghedini, S. 1981, *Societa Astronomica Italiana*, 52, 633.
- Gürol, B. 1994, *Inf. Bull. Var. Stars*, No. 4103.
- Hamme, W. van 1993, *Astron. J.*, 106, 2096.
- Henden, A. A., and Kaitchuck, R. H. 1990, *Astronomical Photometry: A Text and Handbook for the Advanced Amateur and Professional Astronomer*, Willmann-Bell, Richmond.
- Hoffleit, D. 1932, *Bull. Harvard Coll. Obs.*, No. 887, 9.
- Hrivnak, B.J., Guinan, E.F., DeWarf, L. E., and Ribas, I. 2001, *Astrophys. J.*, 121, 1084.
- Jager, C. de and Nieuwenhuijzen, H. 1987, *Astron. and Astrophys.*, 177, 217.
- Kreiner, J.M. 2004, *Acta Astronomica*, 54, 207.
- Kwee, K.K. and Woerden, H. van 1956, *B.A.N.*, 12, 327.
- Lafta, S.J., and Grainger, J. F. 1985, *Astrophys. Space Sci.*, 114, 23.
- Lucy, L.B. 1967, *Z. Astrophys.*, 65, 89.
- Minor Planet Observer 2010, MPO Software Suite, BDW Publishing, Colorado Springs (<http://www.minorplanetobserver.com>).
- Nelson, R. 2005, "Eclipsing Binary O-C," URL: http://www.aavso.org/observing/programs/eclipser/omc/nelson_omc.shtml.
- Nelson, R.H. 2007, "Minima@2002-2006: "Astronomy Software by Bob Nelson" URL: <http://members.shaw.ca/bob.nelson/software1.htm>
- Nelson, R.H. 2009, "WDwint56a: "Astronomy Software by Bob Nelson" URL: <http://members.shaw.ca/bob.nelson/software1.htm>
- Pribulla, T., Gazeas, K and Ogloza, W. 2007, *Astron. J.*
- Prša, A., and Zwitter, T. 2005, *Astrophys J.*, 628, 1, 426.
- Ruciński, S.M. 1969, *Acta Astron.*, 19, 245.
- Ruciński, S.M. 1995, *Acta Astron.*, 49, 341.
- Ruciński, S.M. and Kałużny, J. 1981, *Acta Astron.*, 31, 409.
- Ruciński, S.M., Pribulla, T. and Kerkwijk, M.H. van 2007, *Astron. J.*, 134, 2353.
- Schwarzenberg-Czerny, A. 1996, *Astrophys J.*, 460, L107.
- Wilsey, N.J. and Beaky, M.M. 2009, *Proceedings for the 28th Annual Conference of the Society for Astronomical Sciences*, 107.
- Wilson, R.E. 1979, *Astrophys J.*, 234, 1054.
- Wilson, R.E. 2001, *Inf. Bull. Var. Stars*, No. 5076.
- Wilson, R.E. and Devinney, E.J. 1971, *Astrophys J.*, 166, 605.

In the Next Issue

Photometry of RT LMi, a Short Period Eclipsing Binary with a Split Personality

Complete light curves for RT LMi were collected in B, V and I_C passbands. Roche modeling of this system provided potential solutions as both an A-type and W-type overcontact binary system.

Photometry Basics Part II:

A review of low cost and free software tools for period determination and Roche modeling of light curve data, regression analysis of O-C data, and producing figures.